ACCSCIENCE PUBLISHING

International Journal of Bioprinting

RESEARCH ARTICLE

Three-dimensional-printed bilayered scleral patches with mechano-biological synergistic activity for posterior scleral reinforcement in pathological myopia

Mengdi Chai[1†], Qing He[1†], Tingting Liu[2], Xiu Wang[1], Di Wu[1], Bin Yao[3*], and Ruihua Wei[1*]

[1]Tianjin Key Laboratory of Retinal Functions and Diseases, Tianjin Branch of National Clinical Research Center for Ocular Disease, Eye Institute and School of Optometry, Tianjin Medical University Eye Hospital, Tianjin, China

[2]Department of Laboratory Diagnosis, The 971st Hospital, Qingdao, Shandong, China

[3]Academy of Medical Engineering and Translational Medicine, School of Medicine, Tianjin University, Tianjin, China

[†]*These authors contributed equally to this work.*

***Corresponding authors:**
Ruihua Wei
(rwei@tmu.edu.cn);
Bin Yao
(hongyaobin_1212@tju.edu.cn)

Citation: Chai M, He Q, Liu T, *et al*. Three-dimensional-printed bilayered scleral patches with mechano-biological synergistic activity for posterior scleral reinforcement in pathological myopia. *Int J Bioprint*. 2026;12(5):026240246.
doi: 10.36922/IJB026240246

Received: June 9, 2026

Revised: July 23, 2026

Accepted: August 3, 2026

Published online: August 3, 2026

Copyright: © 2026 Author(s). This is an Open-Access article distributed under the terms of the Creative Commons Attribution License, permitting distribution, and reproduction in any medium, provided the original work is properly cited.

Publisher's Note: AccScience Publishing remains neutral with regard to jurisdictional claims in published maps and institutional affiliations.

Abstract

Pathological myopia (PM) is a leading cause of irreversible vision impairment, characterized by progressive axial elongation and posterior staphyloma. Posterior scleral reinforcement (PSR) surgery is a key intervention to halt disease progression. In this procedure, PSR materials are fixed to the posterior pole of the eye to enhance the original scleral biomechanical properties and promote collagen deposition. However, the materials used for PSR are difficult to obtain and fail to fully achieve all required biomechanical functions. In this study, a novel bilayered biomaterial combining mechanical support with bio-regenerative capacity was developed. A reinforcement layer comprising decellularized porcine sclera (dPS) and an inner functional layer of gelatin methacryloyl/decellularized scleral extracellular matrix (GelMA/dSECM) hydrogel were developed via low-temperature extrusion-based three-dimensional printing. The dPS layer provided stable mechanical support with high tensile strength, while the GelMA/dSECM hydrogel exhibited a porous microstructure. Bioactive components released from the bilayered material enhanced human scleral fibroblast proliferation, migration, and collagen I expression. Bioinformatic analysis revealed that dSECM core proteins were enriched in extracellular matrix organization and angiogenesis-related pathways. In a guinea pig model of form-deprivion myopia, the bilayered material controlled axial elongation and limited increases in vitreous chamber depth. It promoted scleral thickening and achieved close apposition with host tissue within four weeks. This work presents a "mechanical support + regenerative" synergistic system, offering a potential strategy for effective PM management.

Keywords: Myopia; Pathological myopia; Posterior scleral reinforcement; Gelatin methacryloyl; Extracellular matrix

1. Introduction

Myopia has emerged as a global public health concern with a notably rising prevalence, especially in East Asia.[1,2] Pathological myopia (PM) is a progressive form of the disease, defined by severe refractive error (≤ −6.00 D) and axial length (AL) of 26 mm or greater. Driven by its risk of irreversible visual impairment, the growing burden of PM has elevated it to a global public health priority.[3,4] Studies have suggested that PM may be associated with weakened scleral biomechanics and may also involve excessive axial elongation and globe expansion.[5,6] During the progression of PM, vision-threatening retinal complications can occur. These include posterior staphyloma (PS) and retinal traction-related disorders, such as retinoschisis or retinal detachment.[7] PS is a typical manifestation of PM. It is characterized by an irregular bulge of the sclera at the posterior pole. PS exerts a pulling force on the retina, with insufficient elasticity, which increases the risk of traction-related complications.[8] Current treatment strategies suggest that applying external pressure to the eye may be effective for managing PM.[9,10]

Clinically, posterior scleral reinforcement (PSR) has been used for decades to treat PM, reduce AL, and stabilize PM progression.[11] Scleral alterations include reduced collagen fiber diameter and defective fibrillogenesis, which are collectively associated with scleral thinning and localized expansion.[12] PSR strips reinforce the structure by attaching to and thickening the sclera. This promotes the formation of fibrous connective tissue.[13] The transforming growth factor beta (TGF-β) signaling pathway is involved in this process.[14] However, current PSR materials have significant limitations. Biologically derived grafts are currently used, such as allogeneic dura mater, allogeneic dermis, and bovine pericardium.[15,16] They act as passive mechanical reinforcement rather than actively participating in scleral remodeling. Among them, human dura mater (HDM) shows better outcomes and is widely used to control axial elongation.[17,18] However, some patients who undergo PSR still experience a small degree of axial elongation, even with HDM. In addition, HDM is difficult to obtain.[19,20] Therefore, many researchers have studied approaches to overcome these gaps. However, new materials often have drawbacks such as rapid degradation, poor mechanical properties, or insufficient clinical safety.[13,21,22] These limitations highlight the need for a PSR material with adequate biocompatibility, flexibility, and mechanical strength.[17]

Gelatin methacryloyl (GelMA) is a photocrosslinkable biomaterial synthesized through the reaction of gelatin with methacrylic anhydride (MA). It mimics the extracellular matrix (ECM) to support cell adhesion, proliferation, and differentiation, without toxic byproducts.[23] To meet specific tissue requirements, GelMA's tunable structure and porosity can be precisely tuned by crosslinking density, polymer concentration, and curing duration.[24,25] In addition, native tissue-derived ECM contains abundant proteins, including collagen, fibronectin, laminin, and tissue-specific growth factors. Cell–ECM interactions regulate cell function, promote ECM remodeling,[26] and actively participate in tissue regeneration and angiogenesis.[27,28] Decellularized porcine sclera (dPS) closely resembles the human sclera, as the collagen fibers are arranged in dense lamellar bundles. It has been used to repair scleral injuries.[29] Extrusion-based three-dimensional (3D) printing offers fast deposition and printing speeds. It has significant advantages in achieving porous structures, biodegradability, and bioactivity.[30]

Based on this clinical need, we designed a novel bilayered PSR material to achieve simultaneous structural support and biological function. The outer layer is dPS, which provides mechanical reinforcement and resists rapid degradation. The inner layer is a GelMA/decellularized scleral ECM (dSECM) hydrogel, which promotes scleral fibroblast recruitment, collagen deposition, and vascularization. The material was precisely fabricated using extrusion-based 3D printing. The customized inner functional layer was directly deposited onto the outer layer and rapidly crosslinked via visible light to form a bilayered PSR material.

2. Materials and methods

2.1. Materials and equipment

Phosphate-buffered saline (PBS), penicillin–streptomycin, Triton X-100, and sodium dodecyl sulfate (SDS) were obtained from Solarbio (China). GelMA (EFL-GM-60) was purchased from Suzhou Intelligent Manufacturing Research Institute (China). HDM used as the clinical reference was obtained from the Biobank of Tianjin Medical University Eye Hospital (China). Lithium phenyl-2,4,6-trimethylbenzoylphosphinate (LAP) was supplied by Aladdin (China). Collagenase XIV (HY-E70005D) was purchased from MCE (United States). The bicinchoninic acid (BCA) assay kit (P0012S, Beyotime, China), dsDNA HS Assay Kit (12640ES60, Yeasen, China), glycosaminoglycans assay kit (ab289842, Abcam, United States), and collagen type I assay kit (ab285250, Abcam, United States) were used for the study. Hematoxylin and eosin (H&E) stain was purchased from Servicebio (China). Optimal cutting temperature compound was obtained from Sakura (United States). Human scleral fibroblasts (HSFs) and human umbilical vein endothelial cells (HUVEC) were obtained from Warner Biotechnology Co., Ltd. (China). Dulbecco's Modified Eagle Medium

(DMEM), RPMI-1640, fetal bovine serum (FBS), and trypsin were purchased from Gibco (United States). Calcein AM and propidium iodide (PI) were obtained from Solarbio (China). The Cell Counting Kit-8 (CCK-8) assay kit (C0042) was purchased from Beyotime (China). The anti-COL1A1 primary antibody (AB316222) and fluorescein isothiocyanate-conjugated secondary antibody (AB150077) were obtained from Abcam (United States). F-actin was stained with Alexa Fluor 594-conjugated phalloidin (C2205S, Beyotime, China). 4',6-diamidino-2-phenylindole was supplied by Solarbio (China). Matrigel® was purchased from Corning (United States). The low-temperature extrusion-based bioprinter (EFL BP-66) was obtained from Suzhou Intelligent Manufacturing Research Institute (China). The rotational rheometer (MCR302) was purchased from Anton Paar (Austria). The scanning electron microscope (Sigma360) was obtained from ZEISS (Germany). Fluorescence microscopy was performed using an EVOS M5000 (Thermo Fisher, United States). Three-week-old male tricolor guinea pigs were provided by the Laboratory Animal Center of Tianjin Medical University (China).

2.2. Preparation of decellularized porcine sclera

Fresh porcine eyeballs were immersed in PBS containing 1% penicillin–streptomycin and dissected on ice. After removal of the extraocular tissues, the optic nerve was transected, and the eyeball was incised laterally. The intraocular contents, including the vitreous body, lens, retina, and choroid, were carefully removed. The cornea and corneoscleral limbus were excised, and the remaining scleral stromal layer was collected and flattened. The tissues were treated with 0.5% Triton X-100 and 1% SDS under continuous agitation on a low-temperature shaker for 72 hours until the solution became milky white. Samples were washed with pre-cooled PBS, filtered, and embedded in optimal cutting temperature compound for cryosectioning into 100 μm-thick sections. Decellularized scleral sheets were washed in PBS for 24 hours, with solution changes every 6 hours, and stored in 75% ethanol at 4 °C. Decellularization efficiency was verified by H&E staining. The absolute residual dsDNA content was quantified using a dsDNA HS Assay Kit. The total dsDNA was measured with a Qubit fluorometer and normalized to the dry weight of the tissue sample. The absolute residual DNA was calculated using **Equation 1**:

$$\text{Absolute residual dsDNA} = \text{Qubit} \times \text{Total elution volume} \div \text{Dry tissue weight} \quad (1)$$

Glycosaminoglycans and collagen type I were retained and assessed using the respective assay kits.

2.3. Extraction of decellularized scleral extracellular matrix

Porcine scleral tissues were minced into ~2 × 2 mm^2 fragments and decellularized, as described in **Section 2.2**. The decellularized tissue was lyophilized and pulverized into powder. The powder was digested with pepsin in 0.5 M acetic acid under continuous shaking at low temperature until a viscous, translucent solution was formed. The digestate was centrifuged, and the supernatant was collected. The protein concentration was determined using a BCA assay, and the dSECM solution was stored in a gel at −80 °C.

2.4. Fabrication of decellularized porcine sclera/gelatin methacryloyl/decellularized scleral extracellular matrix bilayered biomaterial

Lyophilized GelMA (6% w/v) was dissolved in 5% (w/v) dSECM gel, and the pH was adjusted to 7.2 using 1 M sodium hydroxide. LAP was added as a photoinitiator at 1% (w/v). GelMA/dSECM bioink was loaded into light-protected syringes and printed using a low-temperature extrusion-based bioprinter. The printing parameters were a platform temperature of 4 °C, nozzle temperature of 21 °C–23 °C, nozzle diameter of 350 μm, extrusion pressure of 20 kPa, and printing speed of 100 mm/s. A crosshatched structure with a strand spacing of 1 × 1 mm and a layer thickness of 100 μm was deposited onto a prefabricated dPS outer layer. The construct was photocrosslinked under visible light for 60 seconds to form an integrated bilayer band.

2.5. Material characterization

2.5.1. Mechanical testing

Uniaxial tensile testing was performed using a universal testing machine (AGS-X, Shimadzu, Japan). Rectangular specimens (approximate dimensions: 25 mm × 8 mm; gauge length: 20 mm) were tested in the wet state at 37 °C at a crosshead speed of 1 mm/min, with the loading direction parallel to the long axis of the specimen, until failure (n = 3 per group). The stress–strain curve was recorded. The tensile (secant) modulus was calculated as the secant slope from the origin to the proportional limit (yield point), representing the apparent stiffness of the material within a broader elastic deformation range. The ultimate tensile strength and elongation at break were also measured.

2.5.2. Rheological analysis

Viscoelastic properties were measured using a rotational rheometer with a 25-mm parallel-plate geometry and 0.6

mm gap. Oscillatory frequency sweeps (0.1–10 Hz) were performed at 0.1% strain and 37 °C to record the storage (G') and loss (G") moduli.

2.5.3. Degradation profiling

Cylindrical thin sheets with uniform dimensions were prepared from GelMA, GelMA/dSECM hydrogel, dPS outer layer material, and the dPS/GelMA/dSECM bilayer composite to ensure a comparable surface-area-to-volume ratio. The size was as follows: diameter: 8 mm; homogeneous hydrogel thickness: 1 mm; and total bilayer thickness: approximately 1.1 mm, consisting of a 1.0 mm dPS outer layer and a 0.1 mm printed hydrogel inner layer. The dPS layer thickness of 1.0 mm corresponded to the clinically relevant thickness intended for human application, while the thinner dPS (100 μm) was used in guinea pig implantation due to the anatomical constraints of the small animal model.

The initial dry weight (W_0) of each sample was recorded. To evaluate the barrier function of the dPS outer layer, additional groups consisting of dPS monolayer materials and the dPS/GelMA/dSECM bilayer composite were included. All samples were incubated in PBS (pH 7.4) or PBS containing 1 U/mL collagenase XIV at 37 °C under continuous shaking (150 rpm). The medium was replaced daily to maintain enzymatic activity. At predetermined time points (days 1, 3, 5, 7, and 14), the samples were retrieved, rinsed, freeze-dried (lyophilized), and weighed as the dry weight (W_1). The percentage mass loss was calculated using **Equation 2**:

$$\text{Mass loss} = [(W_0 - W_1)/ W_0] \times 100\% \quad (2)$$

2.5.4. Swelling profiling

To measure the *in vitro* swelling, the dPS, GelMA, GelMA/dSECM hydrogel, and dPS/GelMA/dSECM freeze-dried samples were weighed as W_d; the samples were placed in an appropriate amount of PBS, and after preset time points of 2, 4, 6, 12, 24, and 36 hours, the samples were taken out of the PBS and weighed as W_s after drying the surface. The samples were placed back into PBS after each weighing step, and the swelling degree (%) of the material was calculated using **Equation 3**:

$$\text{Swelling degree} = [(W_s - W_d)/W_d] \times 100\% \quad (3)$$

2.5.5. Microscopic morphology

Lyophilized hydrogel samples were sputter-coated with gold and imaged using scanning electron microscopy to analyze pore morphology and distribution.

2.5.6. Lap shear adhesion test

The interfacial adhesion strength between the dPS layer and GelMA/dSECM hydrogel layer was evaluated using a lap shear test. Briefly, GelMA/dSECM hydrogel (round, 2.0 mm^2) was printed and photocrosslinked onto dPS. The two surfaces of each layer were attached to rigid plastic backing plates using epoxy adhesive. After the adhesive was fully cured, the assembly was mounted on a universal testing machine (WDS-5A) and subjected to tensile loading at a constant crosshead speed of 1 mm/min in the direction parallel to the interface until complete separation occurred. The maximum load was recorded, and the lap shear strength was calculated by dividing the maximum load by the overlapping area (n = 3).

2.6. *In vitro* studies

2.6.1. Human scleral fibroblasts and human umbilical vein endothelial cell culture

Human scleral fibroblasts were maintained in complete culture medium consisting of DMEM with 10% FBS, 1% penicillin–streptomycin, and additional growth factors. HUVECs were cultured in RPMI-1640 complete culture medium supplemented with FBS and penicillin/streptomycin. All the cultures were incubated under standard conditions at 37 °C in a humidified atmosphere containing 5% CO_2. Upon reaching 80% confluence, the cells were passaged or harvested for subsequent experiments using 0.25% trypsin. HUVECs and HSFs were cultured until passage four (P4) for subsequent experiments.

2.6.2. Cytotoxic assay

The GelMA, GelMA/dSECM hydrogel, dPS, and dPS/GelMA/dSECM bilayered materials were placed in the Transwell inserts, whereas the HSFs were seeded in the lower chamber and maintained in complete culture medium. Cell proliferation was quantitatively assessed on days 1, 3, and 5 using the CCK-8 assay, according to the manufacturer's instructions. The absorbance was measured at 450 nm using a microplate reader.

2.6.3. Live/Dead assay

Human scleral fibroblasts were seeded directly onto the surface of the GelMA/dSECM inner layer and dPS outer layer at a density of 5×10^4 cells per well in a 24-well plate and cultured for 1, 5, and 7 days. Cell viability was assessed using a Live/Dead assay based on Calcein AM/PI staining. Briefly, HSFs were incubated in Calcein AM solution for 15 minutes at 37 °C and subsequently washed three times with DMEM. The samples were then treated with PI solution for 10 minutes, followed by three additional

washes with DMEM. Imaging was performed using a fluorescence microscope, wherein viable cells exhibited green fluorescence and nonviable cells displayed red fluorescence.

2.6.4. Migratory behavior by scratch wound assay

The GelMA, GelMA/dSECM hydrogel, dPS, and dPS/GelMA/dSECM bilayered materials were placed in the Transwell insert, respectively, whereas HSFs were seeded in the lower chamber and maintained in complete culture medium. Upon reaching full confluence, a standardized scratch was introduced into the HSF monolayer using a sterile 200 μL pipette tip. The cells were then rinsed gently to remove detached debris and incubated under the same co-culture conditions. Phase-contrast images of the wound area were captured immediately after scratching (0 hour) and at 12 and 24 hours post-scratch using an inverted microscope (Axio Observer, Zeiss, Germany). The migration rate was quantified by measuring the change in wound width using the ImageJ software (version 1.54p), and statistical comparisons were made among the different material groups.

2.6.5. Immunofluorescence staining

Human scleral fibroblasts were cultured on the bottom of the well plates. The GelMA/dSECM hydrogel and dPS were in close contact with the cells in complete medium for 5 days. Immunofluorescence (IF) staining was performed on days 3 and 5 to verify COL1A1 expression. The cells were initially fixed in 4% paraformaldehyde for two hours at room temperature, followed by three PBS washes. Permeabilization was performed using 0.5% Triton X-100 (15 minutes), followed by PBS rinses. After blocking with 0.5% BSA for one hour, the samples were incubated overnight at 4 °C with anti-COL1A1 primary antibody (1:200), followed by incubation with fluorescein isothiocyanate-conjugated secondary antibody (1:150) for four hours at room temperature. After PBS washes, F-actin was stained with Alexa Fluor 594-conjugated phalloidin (1:200) for 30 minutes at room temperature in the dark. Following 4',6-diamidino-2-phenylindole counterstaining (15 minutes) and final PBS washes, the samples were imaged using fluorescence microscopy. Cell–nucleus alignment was quantified using the Directionality plugin in ImageJ. For each image, the plugin computed the spatial orientation distribution of nuclei and provided the preferred angle of alignment for each image.

2.6.6. Tube formation assay

Human umbilical vein endothelial cells (passage 4) were seeded at a density of 2×10^4 cells/well in a 12-well plate pre-coated with Matrigel®. The cells were co-cultured with or without the dPS/GelMA/dSECM bilayer material (control). The material was placed in the upper chamber of a Transwell insert, and the cells were cultured in the lower chamber. After incubation at 37 °C with 5% CO_2 for six hours, tube formation was monitored in real time under a microscope, and images were captured at 2.5, 3, 3.5, and 4 hours. For each well, 2–3 representative fields were manually selected and imaged. Three independent experiments were performed in triplicate. The total number of branching points, tube length, and junction numbers were quantified using ImageJ software with the Angiogenesis Analyzer plugin.

2.7. Proteomic and bioinformatic analysis

2.7.1. Proteomic analysis by liquid chromatography-tandem mass spectrometry

Five parallel dSECM samples were pooled and subjected to proteomic analysis. Proteins were extracted using SDT lysis buffer (4% SDS, 100 mM Tris-HCl, 100 mM DTT, pH 8.0), quantified by the BCA method, and digested with trypsin (Promega, United States) using a commercial protein digestion kit (MMB-96, Qinglian Baiao, China). The resulting peptides were desalted and analyzed using a RIGOL L-3000 high-performance liquid chromatography system coupled to a Q Exactive HF-X mass spectrometer (Thermo Fisher Scientific, United States). Peptides were separated on a C18 analytical column (QL-HPLC-100×15) using a 30-min linear gradient of mobile phase B (80% acetonitrile, 0.1% formic acid) from 8% to 40% at a flow rate of 300 nL/min. The mass spectrometer was operated in data-dependent acquisition mode with the top 40 most abundant precursor ions selected for higher-energy collisional dissociation fragmentation. Full MS scans were acquired at a resolution of 120,000 (at m/z 200) over a range of m/z 350–1500, with an automatic gain control target of 3×10^6 and a maximum injection time of 80 ms. Tandem mass spectrometry scans were acquired at a resolution of 15,000 (at m/z 200) with an automatic gain control target of 5×10^4, a maximum injection time of 45 ms, and a normalized collision energy of 27%. Raw data were searched against the *Sus scrofa* UniProt database (UP000008227, downloaded January 2025, containing 48,909 entries) using Proteome Discoverer 2.4 (Thermo Fisher Scientific, United States). Search parameters included trypsin as the digestion enzyme, a maximum of two missed cleavages, carbamidomethylation of cysteine as a fixed modification, and oxidation of methionine and N-terminal acetylation as dynamic modifications. The precursor mass tolerance was ±15 ppm, and the fragment mass tolerance was ±0.02 Da. Peptide and protein identifications were filtered at a false discovery rate of < 1% at both the peptide spectrum match and protein levels. A total of 28,299 tandem mass

spectrometry spectra were acquired, from which 2,108 unique peptides and 684 proteins were identified.

2.7.2. Gene Ontology and Kyoto Encyclopedia of Genes and Genomes enrichment analysis

Gene Ontology (GO) enrichment analysis, including the categories of biological process, cellular component, and molecular function, and Kyoto Encyclopedia of Genes and Genomes (KEGG) pathway enrichment analysis were conducted using the ClusterProfiler R package (version 4.8.3). The corresponding genes of the identified acellular porcine scleral ECM proteins were analyzed. An adjusted *p*-value (false discovery rate) of < 0.05 was set as the threshold for statistical significance.

2.7.3. Protein–protein interaction network and module identification

The list of acellular porcine scleral ECM proteins was imported into the STRING database (version 11.5) to construct a protein–protein interaction (PPI) network, with a confidence score (minimum required interaction score) set to > 0.7. The resulting network was visualized and analyzed using Cytoscape software (version 3.10.4). The PPI network was clustered using the Molecular Complex Detection plugin in Cytoscape to identify densely connected functional modules. Each module was subjected to an independent KEGG pathway enrichment analysis using ClusterProfiler. The top 25 hub proteins were identified based on degree centrality using the CytoHubba plugin.

2.8. *In vivo* study

2.8.1. Animal model

A total of 45 three-week-old male tricolor guinea pigs with healthy eyes and normal refractive status were used in this study. The experimental protocol was approved by the Ethics Committee of Tianjin Medical University Eye Hospital and complied with the Association for Research in Vision and Ophthalmology Statement for the Use of Animals in Ophthalmic and Vision Research. Animals were randomly assigned to five groups ($n = 9$) using a random number table: (i) dPS/GelMA/dSECM (treated with the bilayered material); (ii) dPS (treated with the dPS outer layer alone); (iii) HDM (treated with clinically used HDM); (iv) form-deprived myopia (FDM; FDM model without surgery); and (v) control (age-matched normal guinea pigs without any intervention). The sample size was determined based on preliminary experimental data. In all treatment groups, myopia was induced by monocular form deprivation using a white balloon over the right eye for 28 days prior to surgery. The contralateral left eye received no intervention. The experimental unit was the individual animal. All biometric measurements were performed by a blinded investigator who was unaware of the group allocation. Exclusion criteria included perioperative infection, intraoperative or postoperative death, implant dislocation, and incomplete data collection; no animals met the exclusion criteria during the study. Guinea pigs were housed in wire-top plastic cages under a 12-hour light/dark cycle, with *ad libitum* access to water and daily vegetable supplementation for dietary enrichment.

2.8.2. Surgical implantation

All surgical procedures were performed under microscopic guidance. Guinea pigs underwent posterior pole subTenon's capsule implantation following inhalation anesthesia. A 10-0 suture was placed to stabilize the posterior scleral access. The surgical protocol included the following: (i) conjunctival and Tenon's capsule incision at the superotemporal and inferotemporal limbal quadrants; (ii) implantation of pre-cut 2 mm square bilayered biomaterials (200 μm total thickness: 100 μm dPS outer layer + 100 μm hydrogel inner layer); and (iii) intermuscular biomaterial placement with equatorial suture fixation. Postoperative care included daily topical application of tobramycin-dexamethasone ointment. All animals survived with 100% surgical success.

2.8.3. Ocular measurements

Ocular parameters were measured at three time points (0, 2, and 4 weeks) in each experimental group. Measurements included refractive error (diopters), AL, anterior chamber depth (ACD), lens thickness (LT), and vitreous chamber depth (VCD). Prior to the measurements, pupil dilation was achieved using three applications of 0.5% tropicamide. Refractive status was determined by subjective retinoscopy, whereas AL, ACD, LT, and VCD were quantified using an MD-1000A ophthalmic ultrasound biometer. These parameters are interrelated as described by **Equation 4**:

$$AL = ACD + LT + VCD \quad (4)$$

2.8.4. Fundus histological staining

Scleral sections (5 μm) from the posterior region of control and FDM eyes were collected at 2- and 4-week post-intervention time points. Tissue samples were sectioned along the vertical meridian and processed for histological analysis using H&E and Masson's trichrome staining protocols.

2.9. Statistical analysis

Statistical analyses were conducted using the Statistical Package for Social Sciences (version 24.0). The normality of data distribution was assessed using the Shapiro–

Wilk test. For pairwise comparisons between two groups that followed a normal distribution, a *t*-test was used. Continuous variables with a normal distribution are expressed as mean ± standard deviation. Between-group differences in baseline characteristics were analyzed using one-way analysis of variance (ANOVA) for normally distributed data. Post-hoc pairwise comparisons were performed using Tukey's HSD test for parametric data, and Dunn's multiple comparison test for non-parametric data (when $p < 0.05$).

Each animal was considered a biological replicate. For each ocular parameter, three consecutive measurements were obtained per eye at each time point, and the average was used for statistical analysis. Continuous variables with normal distribution are expressed as mean ± standard deviation. Baseline differences among groups were evaluated using one-way ANOVA for normally distributed data. To evaluate the effects of treatment over time, a two-way mixed-design ANOVA was performed, with five groups as the between-subjects factor and time (0, 2, and 4 weeks) as the within-subjects (repeated measures) factor; this analysis explicitly tested and reported the main effect of group (between-group differences), the main effect of time (longitudinal changes), and the group × time interaction effect (differential changes among groups over time). Mauchly's test of sphericity was applied; when the sphericity assumption was violated, the Greenhouse–Geisser correction was employed. When a significant main effect or interaction was detected, post-hoc pairwise comparisons were performed using Tukey's test. All tests were twotailed, with statistical significance set at $p < 0.05$. The following notation was used: ns (not significant, $p \geq 0.05$), * ($p < 0.05$), ** ($p < 0.01$), and *** ($p < 0.001$).

3. Results

3.1. Material preparation and three-dimensional bioprinting

3.1.1. Extraction and characterization of decellularized porcine sclera

Porcine scleral tissue was processed to form the dSECM (Figure S1A). The contents of glycosaminoglycan proteins and collagen type I in the dSECM showed no significant changes compared to the native tissue, whereas the dsDNA content was significantly reduced (Figure S1B). The absolute residual dsDNA content in the decellularized porcine sclera was 24.95 ± 7.72 ng/mg dry tissue (n = 3), below the accepted threshold of 50 ng/mg for effective decellularization.[31] H&E staining revealed no noticeable cellular structures in the processed tissues (Figure S1C).

3.1.2. Three-dimensional bioprinting parameter optimization

We systematically optimized hydrogel printability by varying GelMA concentration, curing time, and pore morphology. Among the GelMA concentrations of 4%, 6%, and 10% (w/v), the 6% formulation achieved the most desirable structural integrity with a curing time of 60 s, with biocompatibility when cultured with HSFs (Figure 1A). The optimal crosslinking duration was 60 seconds with 6% concentration (Figure 1B).

Under predetermined printing rate and temperature conditions, a pore size of 1.0 × 1.0 mm yielded the highest printing fidelity. The hydrogel (mixed with blue dye) was directly printed on a low-temperature platform, with the minimal thickness controlled to within 100 μm (Figure 1C and D). The printed structures could be customized to the dimensions required for PSR strips (Figure 1E). Based on the rheological properties of GelMA, printing parameters, including speed and extrusion pressure, were optimized. The results demonstrated that an extrusion pressure of 20 kPa and a printing speed of 100 mm/s, under nozzle temperatures of 21 °C–23 °C and platform temperatures of 4 °C, produced optimal hydrogel morphology (Figure 1F and G). The lap shear adhesion strength between dPS and GelMA/dSECM hydrogel was 24.00 ± 1.73 kPa (Figure 1H). The inner layer exhibited adhesiveness, even when subjected to basic shape changes (Figure 1I).

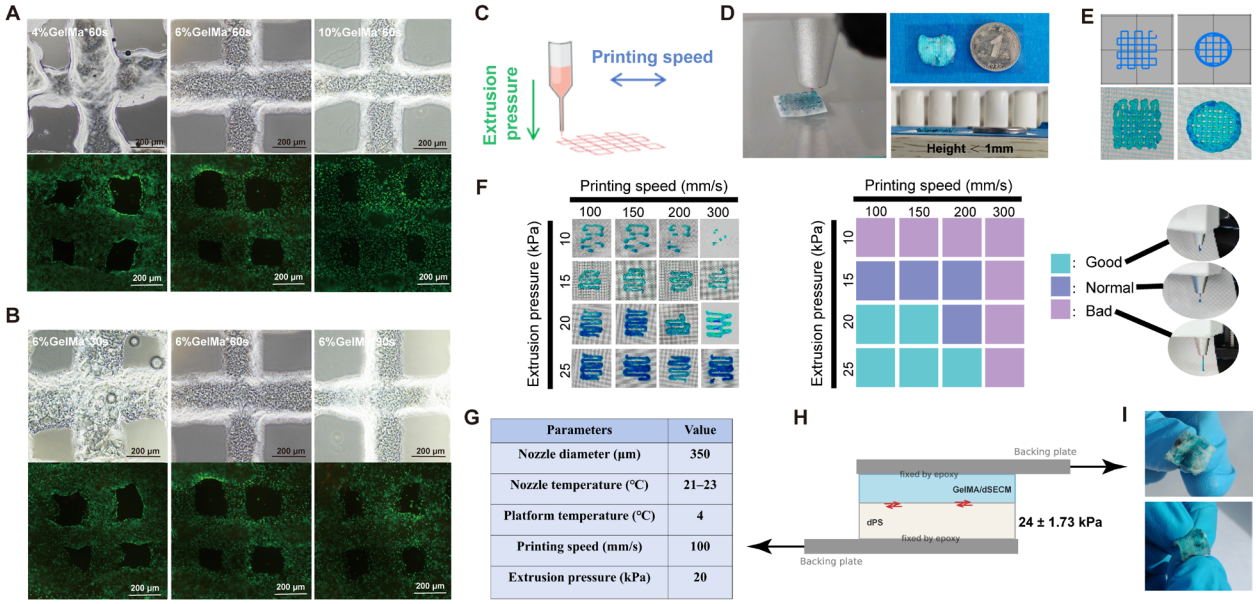
3.2. Material properties

3.2.1. Mechanical performance

The mechanical properties of the dPS/GelMA/dSECM bilayer strips were evaluated and compared with those of HDM, which is currently used in clinical PSR surgery. The stress–strain curves of both dPS/GelMA/dSECM and HDM exhibited typical nonlinear mechanical behaviors (Figure 2A). Because the stress–strain curves of the dPS outer layer and the dPS/GelMA/dSECM bilayer material were highly similar, only the latter is shown in the figure. The tensile modulus of the dPS/GelMA/dSECM group was 6.68 ± 0.48 MPa, showing no significant difference compared to the HDM group (Figure 2B). However, both the dPS/GelMA/dSECM and dPS groups exhibited similar ultimate tensile strengths, measuring 31.46 ± 2.66 MPa and 31.02 ± 1.86 MPa, respectively, which were significantly higher than that of the HDM group (27.81 ± 1.50 MPa; $p < 0.05$) (Figure 2C).

3.2.2. Hydrogel rheological properties and adhesiveness

Frequency sweep tests from 0.1 to 10 Hz at 0.1% strain showed that the storage modulus (G') of all hydrogels



Parameters	Value
Nozzle diameter (μm)	350
Nozzle temperature (°C)	21–23
Platform temperature (°C)	4
Printing speed (mm/s)	100
Extrusion pressure (kPa)	20

Figure 1. Optimization of gelatin methacryloyl/decellularized scleral extracellular matrix (GelMA/dSECM) hydrogel formulation and the optimal printability with morphological characterization. (A, B) Microscopic morphology of three-dimensional (3D) bioprinted hydrogel under different GelMA concentrations (4%, 6%, 10% w/v) and crosslinking durations (30, 60, 90 s) and Live/Dead staining of human scleral fibroblasts cultured on hydrogels after three days. Green: live cells; red: dead cells. Scale bar: 200 μm; magnification: 5×. (C) Schematic of the low-temperature extrusion-based 3D bioprinting process for fabricating the bilayer band. (D) Representative image of the printed hydrogel (blue dye) deposited onto the dPS outer layer. (E) Customized bilayer strips designed for posterior scleral reinforcement, adapted to different cases. (F, G) Effect of extrusion pressure and printing speed on strand continuity and morphology. (H) Lap shear adhesion strength between 2 layers is 25 kPa. (I) During mechanical bending, GelMA/dSECM hydrogel remained adherent to the dPS layer.

remained greater than the loss modulus (G") throughout the frequency range, confirming stable gel states. Figure 2 shows that the measured average G' values are 0.75 kPa for GelMA and 1.84 kPa for GelMA/dSECM. The GelMA/dSECM hydrogel exhibited notable adhesiveness (Figure 2E and F), maintaining tight adhesion even after visible-light curing and morphological reshaping, indicating its high potential for *in vivo* applications.

3.2.3. Swelling and degradation behavior

The swelling ratio of the GelMA/dSECM hydrogels was higher than that of pure GelMA (Figure 2D). The degradation behavior of the dPS/GelMA/dSECM bilayer material was modulated in both collagenase XIV and PBS. In collagenase XIV, pure GelMA exhibited a degradation rate of 94.7% after seven days, whereas the GelMA/dSECM group showed a reduced degradation rate of 87.0%, indicating that the incorporation of dSECM enhanced the material's resistance to enzymatic degradation (Table S1; Figure 2G and H).

3.2.4. Microstructural characterization

A porous structure was observed in the freeze-dried GelMA and GelMA/dSECM hydrogels, with a uniform pore size distribution and good channel connectivity, whereas dPS exhibited a rough surface with visible collagen fibers (Figure 2I). Pore size analysis revealed that dSECM incorporation significantly increased the average pore size in GelMA scaffolds from 36.22 ± 13.60 μm to 110.74 ± 18.49 μm (Figure 2J).

3.3. In vitro functional performance

3.3.1. Proliferation and migration capacity

We established a Transwell culture system containing HSFs with the following materials: GelMA hydrogel, GelMA/dSECM hydrogel, dPS outer layer, and dPS/GelMA/dSECM bilayer material, immersed in complete medium (Figure 3A). On day 5, the absorbance of the dPS/GelMA/dSECM group was significantly higher than that of the GelMA and GelMA/dSECM groups ($p < 0.001$), indicating a synergistic proliferation effect of the bilayer structure (Figure 3B). Scratch assay results demonstrated that incorporating dSECM and dPS significantly enhanced cell migration within 24 hours. The migration rate of the dPS/GelMA/dSECM bilayer group was 71.92% within 12 hours and 93.52% within 24 hours, which was significantly higher

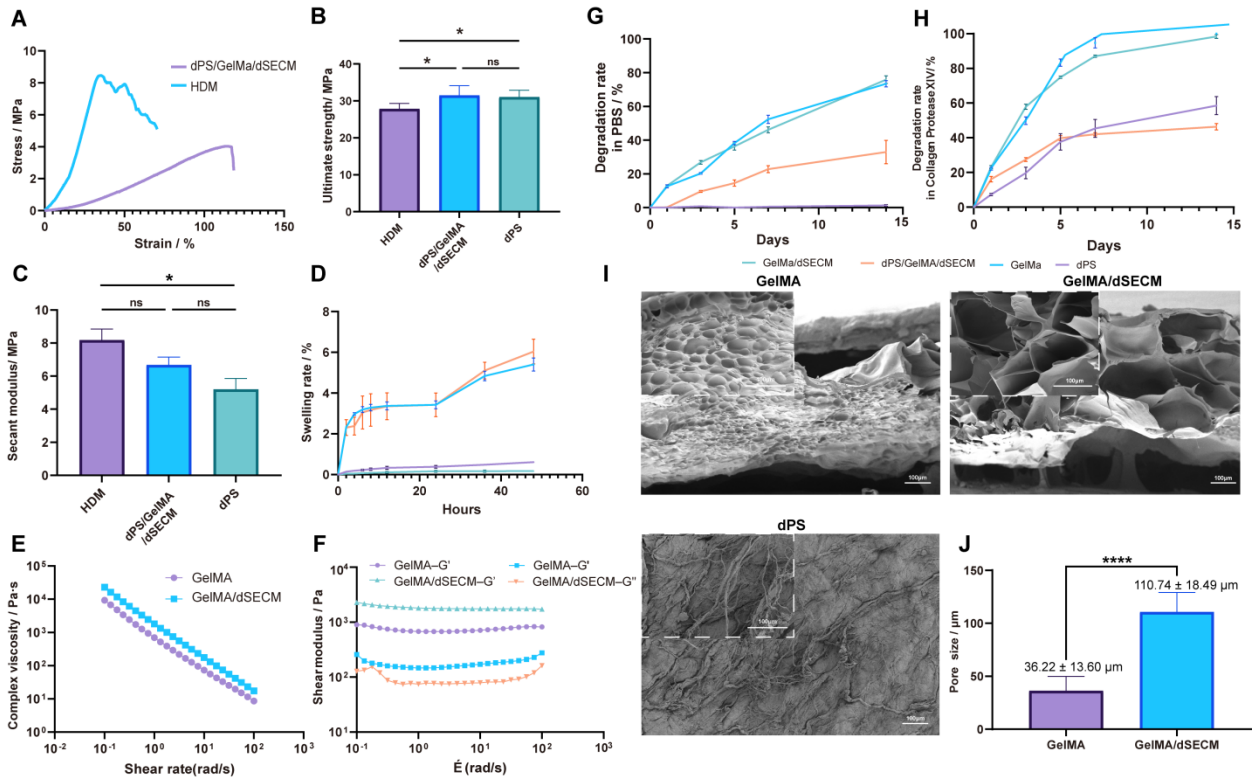


Figure 2. Comprehensive characterization of the mechanical, rheological, and degradation properties of the materials. (A) Representative stress–strain curves of dPS/GelMA/dSECM and HDM bands. (B) Ultimate tensile strength (UTS) and (C) tensile (secant) modulus of the different material groups. (D) In vitro swelling profiles of the different materials. (E) Adhesion test demonstrating the binding stability between the hydrogel layer and dPS substrate after curing and reshaping. (F) Storage (G') and loss (G") moduli of GelMA and GelMA/dSECM hydrogels under frequency sweep. (G) *In vitro* degradation profiles of different materials in PBS and (H) collagenase XIV solution over 14 days. (I) SEM micrograph of dPS, pure GelMA, and GelMA/dSECM hydrogels. Scale bar: 100 μm; magnification: 500×, 200×. (J) Pore size and interconnectivity of GelMA and GelMA/dSECM hydrogels. Data are presented as mean ± standard deviation. Statistical significance was determined by one-way ANOVA with Tukey's post-hoc test. Statistical significance is indicated by asterisks: $^{*}p < 0.05$, $^{**}p < 0.01$, $^{***}p < 0.001$.

Abbreviations: ANOVA: Analysis of variance; dPS: Decellularized porcine sclera; dSECM: Decellularized scleral extracellular matrix; GelMA: Gelatin methacryloyl; HDM: Human dura mater; PBS: Phosphate-buffered saline; SEM: Scanning electron microscopy; UTS: Ultimate tensile strength.

than that of the dPS reinforcement layer alone (66.77% at 12 hours and 89.71% at 24 hours) (Figure 3C and D).

3.3.2. Cytocompatibility of material

The cytocompatibility of the dPS outer layer and GelMA/dSECM hydrogels was assessed using *in vitro* cell culture. HSFs maintained high viability throughout the 7-day culture period, with minimal dead cells. On day 1, the cell confluence reached approximately 30%. By day 5, proliferation had advanced to approximately 80% confluence, accompanied by the formation of multilayered cell clusters within the three-dimensional hydrogel matrix. On day 7, the confluence exceeded 90% with sustained proliferative activity and high cellular viability (Figure 3E and F).

3.3.3. In vitro capillary-like tube formation

Human umbilical vein endothelial cells were cultured with or without dPS/GelMA/dSECM bilayer material to assess its effect on tube formation. The dPS/GelMA/dSECM group exhibited accelerated and more extensive capillary-like structure formation on Matrigel compared with the control (HUVECs alone; Figure 3G). Quantitative analysis confirmed significant increases in total branching points, tube length, and junction numbers in the dPS/GelMA/dSECM group relative to the control (Figure 3H-J).

3.3.4. Promotion of collagen expression and alignment

Human scleral fibroblasts were tightly contacted with dPS and GelMA/dSECM hydrogels for 3 and 5 days

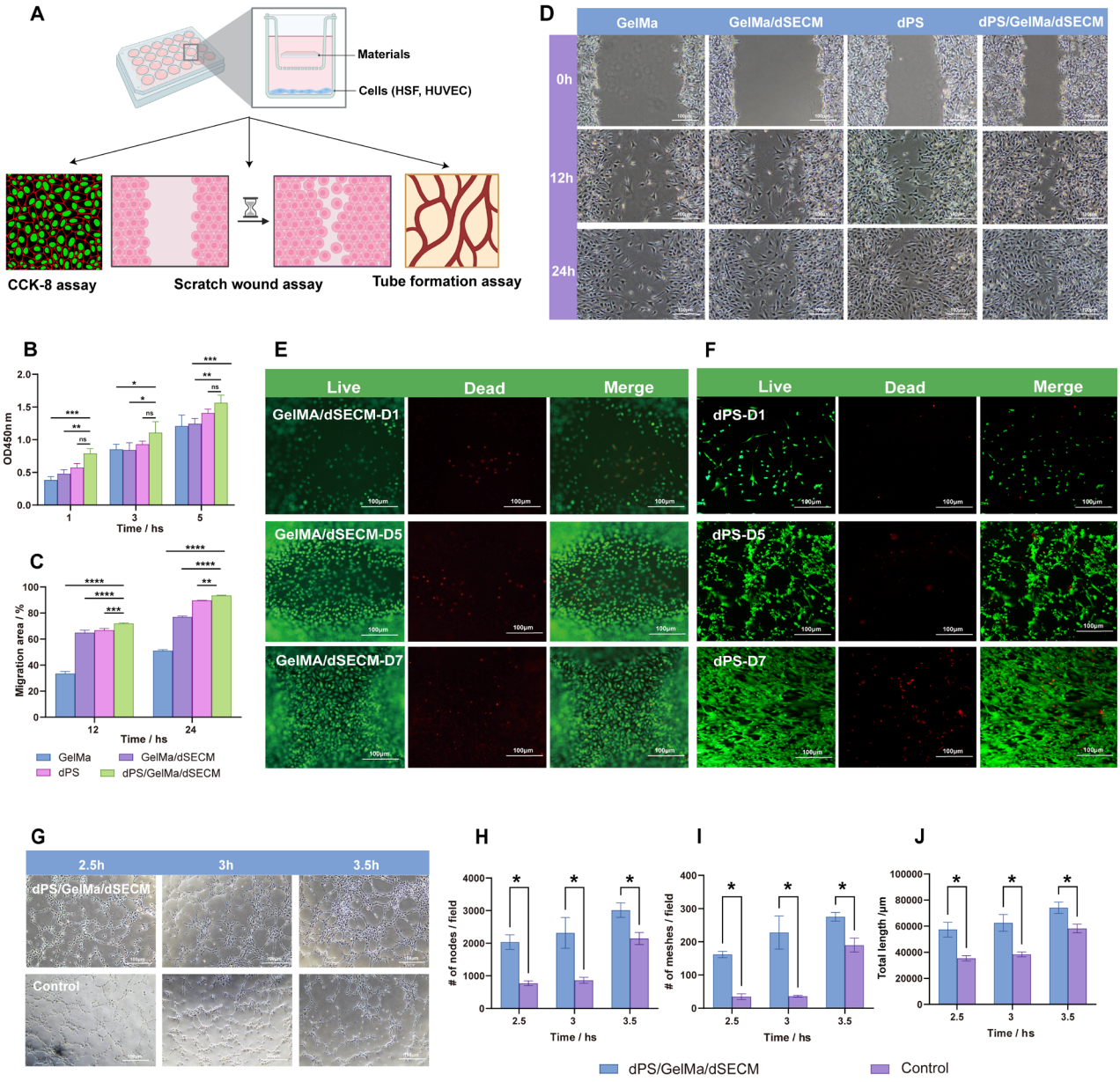


Figure 3. HSFs and HUVECs co-cultured by Transwell with dPS/GelMA/dSECM, showing favorable biocompatibility and promoting cell proliferation, migration, and capillary-like tube formation. (A) Schematic diagram of co-culture of cells with dPS/GelMA/dSECM material. (B) CCK-8 assay quantifying HSF proliferation at 1, 3, and 5 days. (C) Statistical analysis showing HSF migration rates assessed by scratch wound assay. (D) Scratch wound assay of HSF co-cultured with different materials at 12 and 24 hours. Scale bar: 100 μm; magnification: 10×. (E, F) The biocompatibility of GelMA/dSECM hydrogel and dPS with HSF co-culture in 1, 5, and 7 days. Scale bar: 100 μm; magnification: 10×. (G) Representative images of tube formation by HUVECs. Scale bar: 100 μm; magnification: 10×. (H–J) Quantitative analysis of total branch points, tube length, and junction numbers. Statistical significance was determined by one-way ANOVA with Tukey's post-hoc test. Statistical significance is indicated by asterisks: $^{*}p < 0.05$, $^{**}p < 0.01$, $^{***}p < 0.001$.
Abbreviations: ANOVA: Analysis of variance; CCK-8: Cell Counting Kit-8; dPS: Decellularized porcine sclera; dSECM: Decellularized scleral extracellular matrix; GelMA: Gelatin methacryloyl; HSFs: Human scleral fibroblasts; HUVEC: Human umbilical vein endothelial cell; PBS: Phosphate-buffered saline.

(Figure 4A). By day 3, the cell density reached 30%–40%, with detectable expression of type I collagen (COL1A1). By day 5, the GelMA/dSECM inner layer significantly enhanced COL1A1 expression, as indicated by green fluorescence, compared to the dPS outer layer (10 z×) (Figure 4B). Quantitative evaluation confirmed that

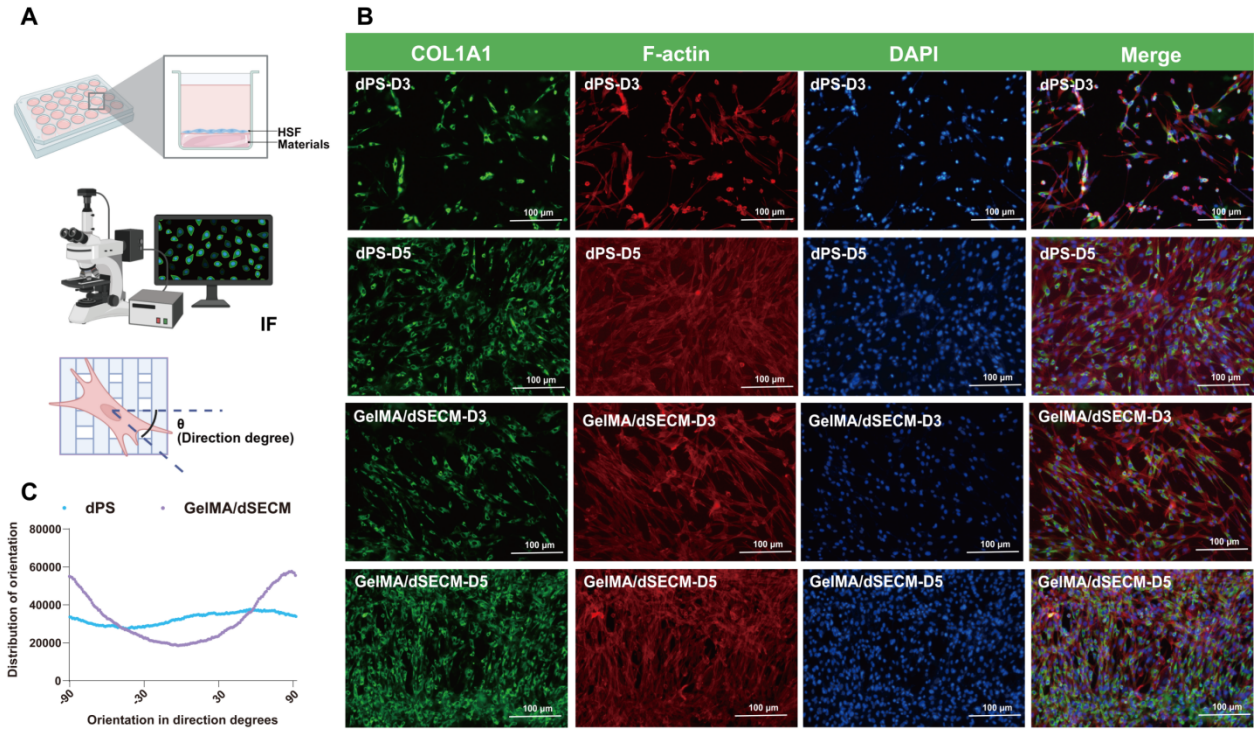


Figure 4. HSFs were closely co-cultured with the dPS outer layer and the GelMA/dSECM hydrogel inner layer, respectively. These co-cultures demonstrated collagen expression and alignment induced by the inner GelMA/dSECM hydrogel. (A) Sketch map showing the close co-culture of HSFs with the material. The method for measuring cell directionality is illustrated. (B) Immunofluorescence staining of COL1A1 (green) and F-actin (red) in HSFs cultured on the dPS outer layer or the inner GelMA/dSECM hydrogel. Images were taken on days 3 and 5. Scale bar: 100 μm; magnification: 10×. (C) Directionality analysis showing the alignment of collagen fibers and cells relative to the printing axis.
Abbreviations: dPS: Decellularized porcine sclera; dSECM: Decellularized scleral extracellular matrix; GelMA: Gelatin methacryloyl; HSFs: Human scleral fibroblasts.

cell orientation (stained for nuclei in blue) and collagen deposition (green) exhibited near-parallel alignment to the printed microstructure. These results indicate that the structural cues provided by the hydrogel can effectively guide the anisotropic deposition of extracellular matrix, underscoring the potential of material design in directing tissue regeneration (Figure 4C).

3.4. Bioinformatic analysis of core functional network in decellularized scleral extracellular matrix proteome

To systematically decipher the biological characteristics of dSECM, we performed an integrated bioinformatics analysis of the data. The results revealed consistent enrichment of pathways centered on ECM construction and angiogenesis-related regulation.

3.4.1. Macro-functional overview: Core theme and extracellular matrix-related proteins

Gene Ontology and KEGG enrichment analyses of all identified proteins were conducted to define the macro-functional landscape. In biological process, the most significantly enriched terms were directly related to "extracellular matrix organization," "extracellular structure organization," and "external encapsulating structure organization." For cellular component, proteins were predominantly localized to the "collagen-containing extracellular matrix" and "focal adhesion." Regarding molecular function, the dSECM proteome was notably enriched in "extracellular matrix structural constituent," "actin binding," and "structural constituent of ribosome." KEGG pathway analysis further revealed significant enrichment in "cytoskeleton in muscle cells" and "regulation of actin cytoskeleton," underscoring the dSECM's inherent capacity for high-level protein synthesis and folding (Figure 5A). These 121 core ECM-related proteins were identified, and the top 25 most abundant proteins were identified (Figure 5B).

3.4.2. Core protein module collaboration and hub protein identification

To understand the collaborative functions within the

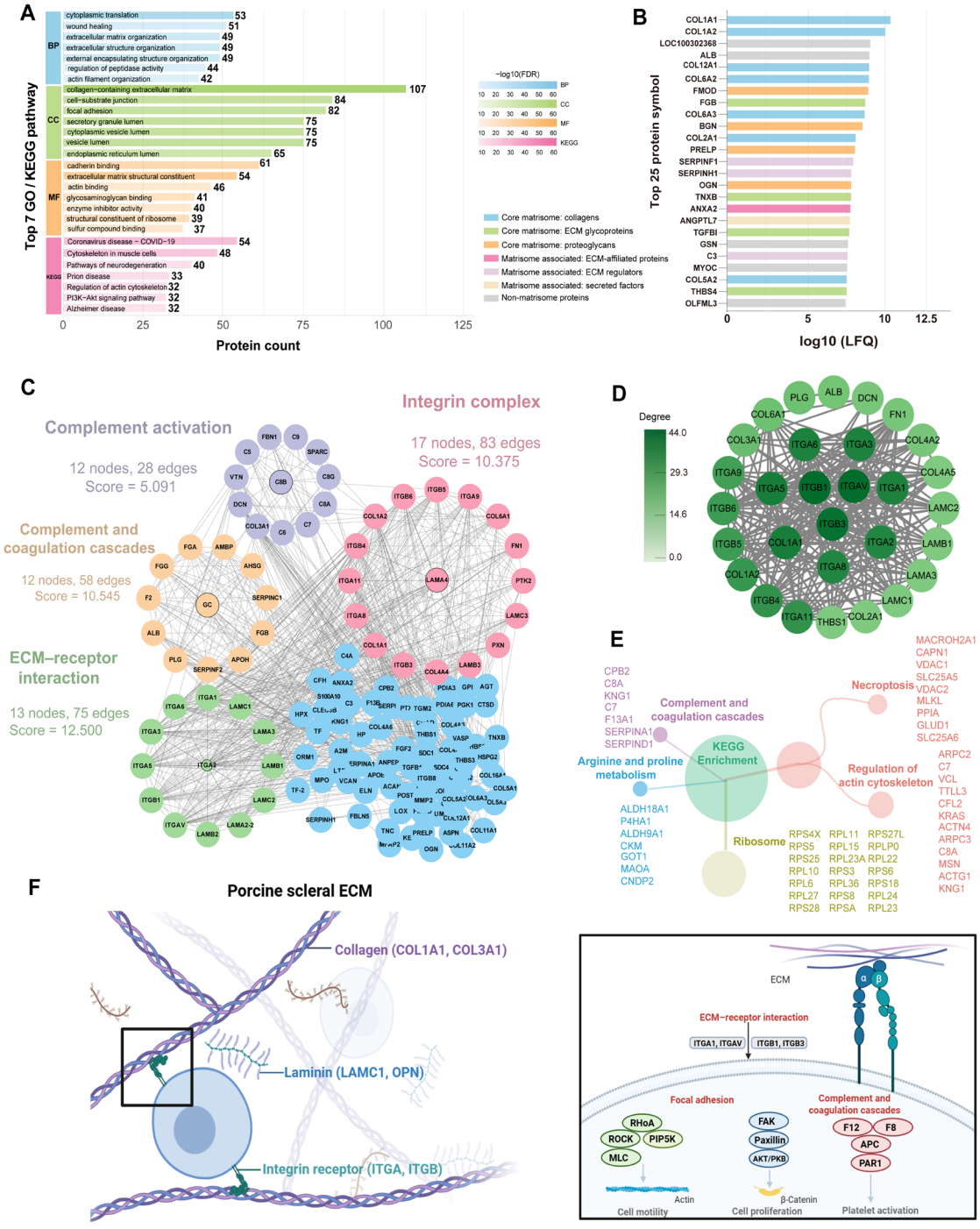


Figure 5. Bioinformatic analysis of the dSECM proteome. (A) GO enrichment analysis across three categories: biological process (BP), cellular component (CC), and molecular function (MF), and KEGG enrichment analysis. (B) Top 25 core proteins of ECM-related proteins. (C) A protein–protein interaction (PPI) network of 121 core proteins was constructed, and functional module analysis was performed, clustering them into four functional modules. (D) Identification of hub proteins in the PPI network by degree centrality, a measure of connectivity within the network. (E) KEGG hierarchy network, visualizing the core enriched KEGG pathways and their functional genes. (F) Proposed mechanism of dSECM bioactivity.

Abbreviations: BP: Biological process; CC: Cellular component; dSECM: Decellularized scleral extracellular matrix; ECM: Extracellular matrix; GO: Gene Ontology; KEGG: Kyoto Encyclopedia of Genes and Genomes; MF: Molecular function.

core matrisome, a PPI network of 121 proteins was constructed and clustered. The analysis revealed four significant functional modules (Figure 5C). Module 1 (score: 12.50, 13 nodes) was primarily enriched in the "receptor interaction" pathway. Module 2 (score: 10.545, 12 nodes) was significantly associated with "complement and coagulation cascade" pathways. Bridging proteins, such as integrin alpha 2 and vitamin D-binding protein, were identified as key nodes connecting different modules, suggesting their role in coordinating the crosstalk between these functional programs. From the PPI network, the top 25 hub proteins were identified based on degree centrality (Figure 5D). Based on hub proteins, the KEGG hierarchy network was used to visualize the core enriched in "regulation of actin cytoskeleton," "ribosome," and "complement and coagulation cascades," according to their functional genes (Figure 5E).

3.4.3. Proposed mechanism of decellularized scleral extracellular matrix bioactivity

Integrating all the findings, we proposed a coherent mechanism for dSECM bioactivity (Figure 5F). It provides a dual signal: first, a structural scaffold via abundant collagen (COL1A1, COL3A1), laminin subunit gamma-1, and osteopontin for ECM construction; and second, bioactive regulatory signals through its hub integrins (integrin alpha V and integrin beta-1) and angiogenic regulators, which synergistically activate core pathways like "ECM–receptor interaction," "focal adhesion," and "complement and coagulation cascades" to direct cellular processes toward ECM remodeling and vascularization.

3.5. In vivo evaluation of pathological myopia progression

3.5.1. In vivo functional evaluation

To evaluate the efficacy of the dPS/GelMA/dSECM bilayer material in controlling myopia progression, we established an FDM guinea pig model (Figure 6A and B). Changes in refractive error, AL, and dynamic alterations in ocular structural parameters were monitored over the postoperative four weeks (Figure 6C). Two-way mixed-design ANOVA revealed significant main effects of group, time, and group × time interaction for refractive error, VCD, AL, and ACD (all $p < 0.001$) (Tables 1 and S2). At four weeks, the refraction in the dPS/GelMA/dSECM group was −1.40 ± 0.55 D, showing no significant difference compared with the dPS group (−1.33 ± 0.41 D) or the HDM group (−1.50 ± 0.55 D), but was significantly better than that of the FDM Control group (−3.71 ± 0.49 D) (all $p < 0.001$) (Table 1, Figure 6D).

No significant differences were observed in ACD or LT among the groups. However, at four weeks post-operation, LT in the FDM control group was significantly greater than that in the control group ($p < 0.05$) (Table 1, Figure 6E and F). At weeks 2 and 4, the FDM control group showed a significant increase in VCD compared with the control group ($p < 0.001$) (Table 1, Figure 6G). At four weeks post-operation, VCD was 3.24 ± 0.13 mm in the dPS/GelMA/dSECM group and 3.29 ± 0.06 mm in the dPS group, which was significantly lower than that in the HDM group (3.48 ± 0.07 mm) and the FDM group (3.59 ± 0.09 mm; $p < 0.01$). The dPS/GelMA/dSECM group exhibited significantly shorter AL (7.90 ± 0.21 mm) compared with the HDM group (8.41 ± 0.17 mm; $p < 0.001$) and the FDM control group (8.55 ± 0.21 mm; $p < 0.001$), while no significant difference was detected between dPS/GelMA/dSECM and dPS groups ($p = 0.852$) (Table 1, Figure 6H). Of note, the dPS/GelMA/dSECM group showed significant AL control as early as week 2 compared with the FDM control group ($p = 0.036$), whereas the dPS group did not reach statistical significance at this time point ($p = 0.060$) (Table 1, Figure 6H). Between-group differences are reported in Table S3.

3.5.2. In vivo structural evaluation

Histological staining revealed scleral morphology under the different treatments. After four weeks of induction, H&E and Masson's trichrome staining showed a significantly loosened scleral structure compared to that in the control (Figure 7A). Although the overall scleral thickness increased in the FDM group (indicated by yellow arrows), it was not associated with enhanced mechanical support. Following PSR with different materials, the sclera appeared markedly denser than that in the FDM group, although variations in thickness were observed (Figure 7B). In the dPS/GelMA/dSECM group, the sclera was substantially thickened, and the implant became closely apposed to and continuous with the host collagen fibers (blue), suggesting progressive tissue incorporation. In contrast, the dPS group showed the formation of new collagen tissue (blue) and vessel-like luminal structures, although the arrangement was disorganized. The HDM group exhibited dense sclera with an implant (pink) accumulating on the outer scleral surface without effective tissue fusion. Statistical analysis of scleral thickness confirmed that the dPS/GelMA/dSECM group (208.33 ± 5.51 μm) was significantly greater than both the HDM and dPS groups ($p < 0.05$) (Figure 7C).

We further documented the temporal morphological changes at 1, 2, and 4 weeks after dPS/GelMA/dSECM implantation in the FDM animals. At week 1, the implant closely adhered to the native sclera with prominent deposition of collagen I (blue) in the periphery, although the structure remained loose and disorganized. Inflammatory cells (red) were visible within the collagen

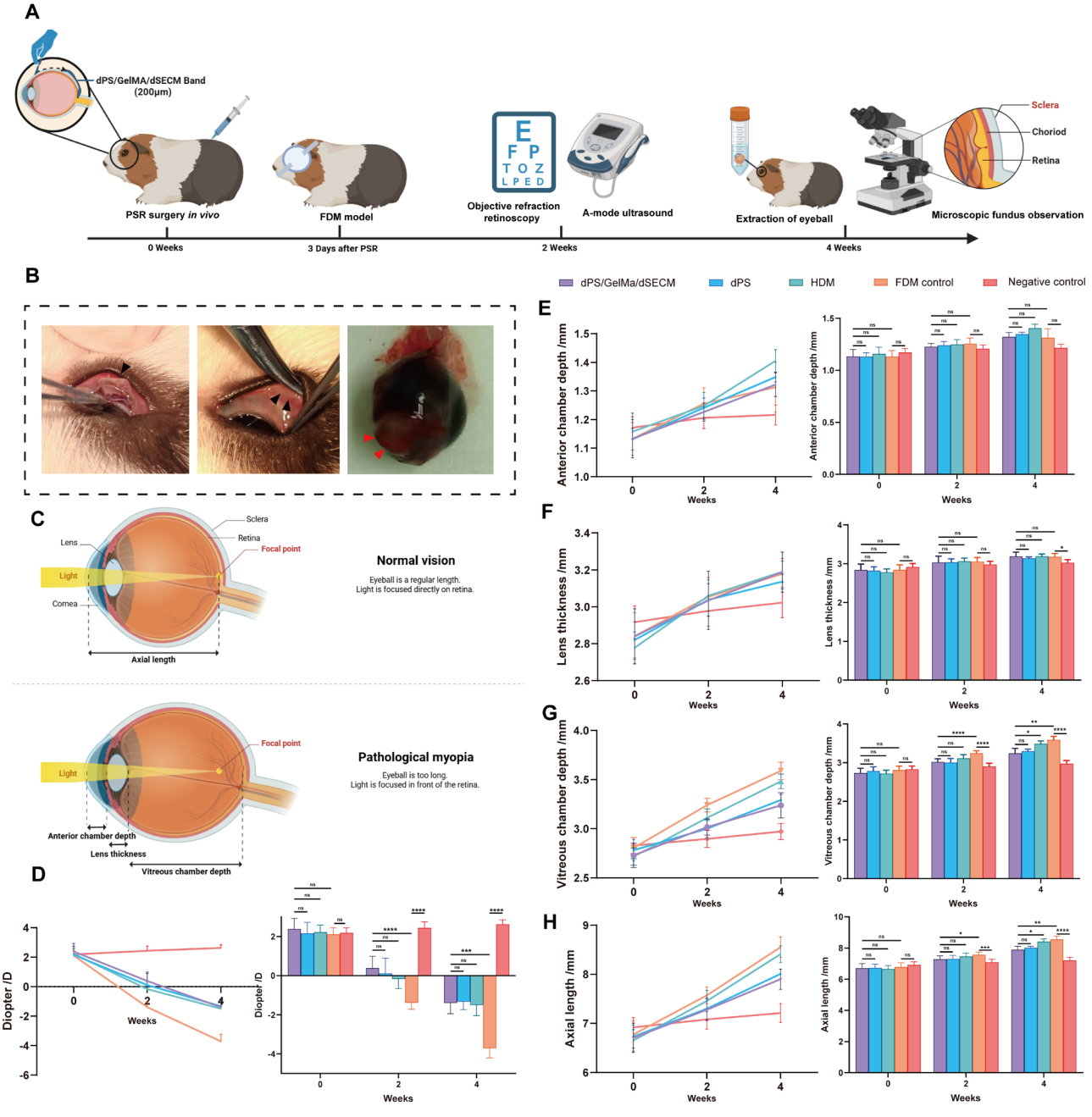


Figure 6. *In vivo* evaluation of myopia control in form-deprived myopia (FDM) guinea pigs. (A) Schematic diagram of the experimental timeline. (B) Representative images of key surgical procedures. Stereoscopic ocular morphology post-surgery is shown in (B), with the red arrow indicating the entire eyeball. (C) Schematic illustration of the key ocular biometric parameters measured. (D–H) Quantitative analysis of ocular parameters across different groups over time: (D) refractive error, (E) anterior chamber depth (ACD), (F) lens thickness (LT), (G) vitreous chamber depth (VCD), and (H) axial length (AL). Statistical significance was determined by repeated-measures ANOVA with Tukey's post-hoc test. Statistical significance is indicated by asterisks: $^{*}p < 0.05$, $^{**}p < 0.01$, $^{***}p < 0.001$.

Table 1. Ocular biometric parameters in different treatment groups

Group	Week 0	Week 2	Week 4	ANOVA
Diopter (D)				
dPS/GelMA/dSECM	2.389 ± 0.546 [a]	0.389 ± 0.601 [b]	−1.400 ± 0.548 [b]	Group: *** Time: *** Group × Time: ***
dPS	2.167 ± 0.559 [a]	0.111 ± 0.782 [b]	−1.333 ± 0.408 [b]	
HDM	2.222 ± 0.363 [a]	−0.167 ± 0.500 [b]	−1.500 ± 0.548 [b]	
FDM control	2.111 ± 0.333 [a]	−1.389 ± 0.333 [c]	−3.714 ± 0.488 [c]	
Control	2.188 ± 0.259 [a]	2.438 ± 0.320 [a]	2.625 ± 0.231 [a]	
ACD (mm)				
dPS/GelMA/dSECM	1.133 ± 0.067 [a]	1.227 ± 0.032 [a]	1.322 ± 0.041 [a]	Group: *** Time: *** Group × Time: ***
dPS	1.131 ± 0.038 [a]	1.241 ± 0.034 [a]	1.348 ± 0.017 [a]	
HDM	1.158 ± 0.065 [a]	1.248 ± 0.047 [a]	1.405 ± 0.039 [a]	
FDM control	1.132 ± 0.057 [a]	1.256 ± 0.055 [a]	1.313 ± 0.087 [b]	
Control	1.171 ± 0.038 [a]	1.206 ± 0.038 [a]	1.216 ± 0.035 [c]	
LT (mm)				
dPS/GelMA/dSECM	2.840 ± 0.150 [a]	3.034 ± 0.158 [a]	3.188 ± 0.109 [a]	Group: ns Time: *** Group × Time: *
dPS	2.820 ± 0.099 [a]	3.038 ± 0.087 [a]	3.137 ± 0.040 [a]	
HDM	2.778 ± 0.086 [a]	3.060 ± 0.086 [a]	3.190 ± 0.059 [a]	
FDM control	2.841 ± 0.126 [a]	3.053 ± 0.106 [a]	3.179 ± 0.082 [a]	
Control	2.916 ± 0.089 [a]	2.978 ± 0.083 [a]	3.022 ± 0.082 [b]	
VCD (mm)				
dPS/GelMA/dSECM	2.730 ± 0.124 [a]	3.017 ± 0.081 [b]	3.238 ± 0.129 [b]	Group: *** Time: *** Group × Time: ***
dPS	2.782 ± 0.107 [a]	3.001 ± 0.105 [b]	3.293 ± 0.056 [b]	
HDM	2.717 ± 0.087 [a]	3.110 ± 0.092 [b]	3.483 ± 0.074 [a]	
FDM control	2.804 ± 0.106 [a]	3.241 ± 0.069 [a]	3.590 ± 0.089 [a]	
Control	2.829 ± 0.083 [a]	2.896 ± 0.087 [c]	2.971 ± 0.083 [c]	
AL (mm)				
dPS/GelMA/dSECM	6.706 ± 0.298 [a]	7.278 ± 0.221 [b]	7.900 ± 0.206 [b]	Group: *** Time: *** Group × Time: ***
dPS	6.731 ± 0.237 [a]	7.299 ± 0.226 [a]	8.010 ± 0.097 [b]	
HDM	6.654 ± 0.218 [a]	7.457 ± 0.217 [a]	8.412 ± 0.170 [a]	
FDM control	6.774 ± 0.275 [a]	7.572 ± 0.172 [a]	8.554 ± 0.209 [a]	
Control	6.919 ± 0.201 [a]	7.080 ± 0.202 [b]	7.210 ± 0.194 [c]	

Note: Data presented as mean ± standard deviation. Two-way mixed-design analysis of variance (ANOVA) and Tukey's HSD test. *p<0.05, ***p<0.001; ns=no significant. [a,b,c]Tukey HSD post-hoc groupings at each time point. Groups sharing the same letter are not significantly different ($p \geq 0.05$), while groups with no shared letter are significantly different ($p < 0.05$). Abbreviations: ACD: Anterior chamber depth; AL: Axial length; dPS: Decellularized porcine sclera; dSECM: Decellularized scleral extracellular matrix; FDM: Form-deprived myopia; GelMA: Gelatin methacrylate; HDM: Human dura matter; LT: Lens thickness; VCD: Vitreous chamber depth.

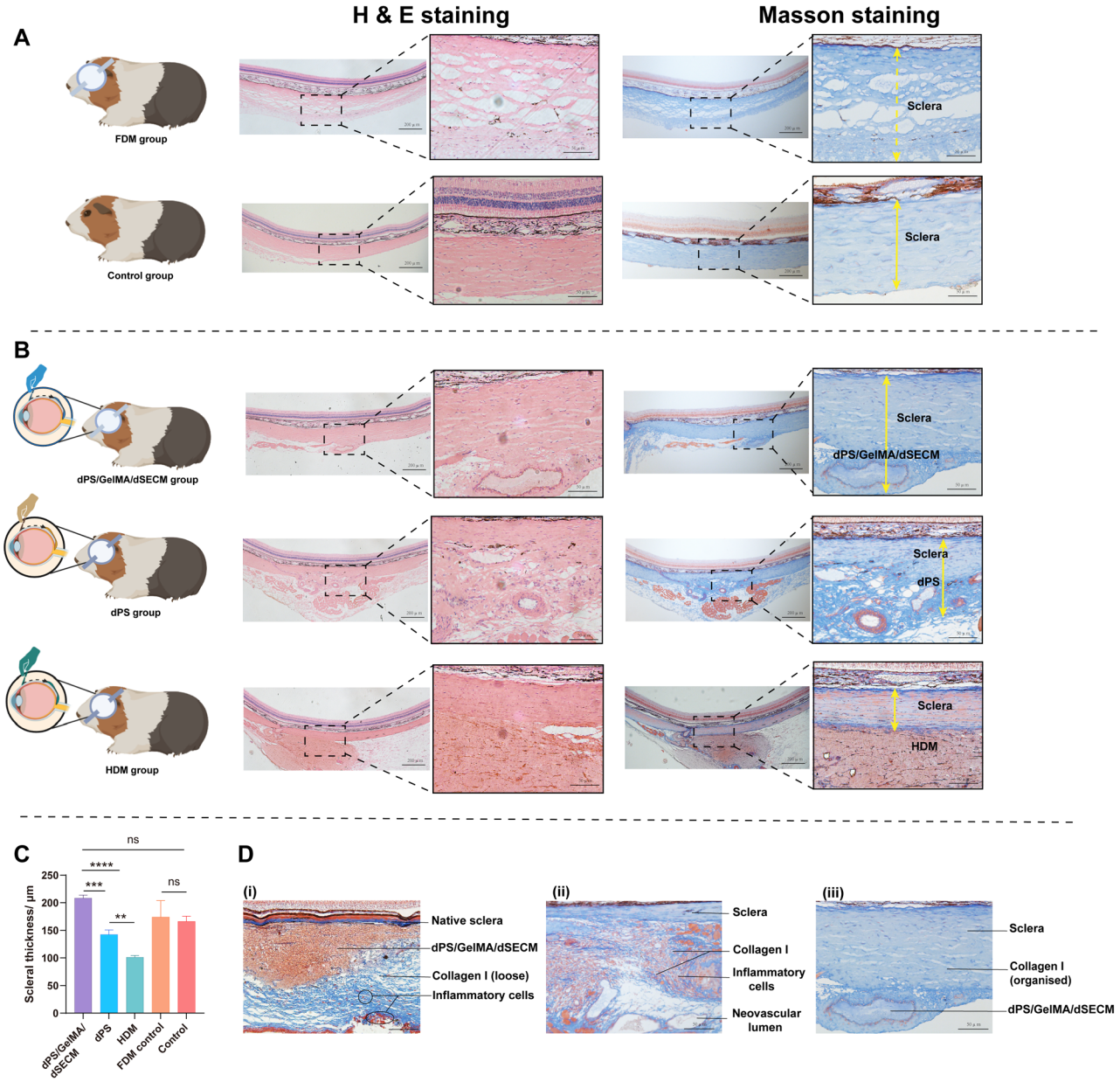


Figure 7. Histological evaluation of scleral tissue response and the implant–tissue interface using hematoxylin and eosin (H&E) and Masson's trichrome staining. (A) Representative images of scleral morphology in the negative control and FDM control groups after four weeks covering the corresponding eye. Yellow arrows indicate scleral thickness. (B) Scleral morphology and implant status at four weeks post-implantation with dPS/GelMA/dSECM, dPS, and HDM in FDM models. Yellow arrows indicate scleral thickness. Scale bars: 50 μm, 200 μm; magnifications: 20×, 4×. (C) Quantitative statistical analysis of scleral thickness. (D) Temporal progression of scleral morphology at the implant–tissue interface at (i) 1, (ii) 2, and (iii) 4 weeks after dPS/GelMA/ dSECM implantation. Key structural features are annotated in the corresponding panels. Scale bar: 50 μm; magnification: 20×.
Abbreviations: dPS: Decellularized porcine sclera; dSECM: Decellularized scleral extracellular matrix; FDM: Form-deprived myopia; GelMA: Gelatin methacrylate; HDM: Human dura matter.

matrix. After two weeks, scleral thickening was evident along with contact with the collagen fibers. New blood vessels began to form adjacent to the implants. At week 4, the sclera was significantly thickened, with regularly organized collagen tissue. These vessel-like structures were no longer apparent, and the implant showed progressive fusion with collagen, becoming incorporated into the scleral structure (Figure 7D).

There was no abnormal inflammatory response in the main organs at eight weeks after subcutaneous implantation of dPS/GelMA/dSECM in the guinea pigs (Figure S2).

4. Discussion

The core pathological changes in the PM include posterior scleral thinning and reduced collagen density, which contribute to progressive axial elongation. Weakened scleral biomechanics are considered key drivers in the progression of high myopia.[5] In PSR surgery, the therapeutic effect depends on the material properties and the surgeon's experience. Previous materials exhibit suitable mechanical strength to achieve mechanical reinforcement. Hui *et al.*[21] reported a GelMA–poly(ethylene glycol) diacrylate hydrogel loaded with fibroblasts. This material enhanced local collagen deposition in the sclera. However, from the perspective of PSR surgery, its degradation rate and mechanical properties did not meet clinical needs. Xu *et al.*[13] reported the experimental effects of a robust silk fibroin hydrogel in rabbits. However, its mechanical properties and biological functions were not evaluated. Zhong *et al.*[22] developed a wireless and battery-free ocular regulation patch. However, its 22-day observation period requires further validation. Jiang *et al.*[32] integrated polyvinylidene fluoride onto the surface of a bovine pericardium patch using a spin-coating technique. This material provides microcurrent stimulation and enhances interaction with the sclera. However, the potential safety effects of electrical stimulation on the retina and optic nerve need further discussion. Thus, the bilayer design establishes a "mechanical support + regenerative" synergistic system: the dPS layer provides mechanical support. Meanwhile, the inner GelMA/dSECM hydrogel recruits scleral fibroblasts, deposits new collagen, and promotes the biological function of the native sclera.

Human natural sclera exhibits viscoelastic nonlinear behavior; when the loading strain rate increases from 10 mm/min to 600 mm/min, the ultimate stress varies from 2.51 MPa to 4.3 MPa.[33] The elastic modulus of the sclera differs across regions, with the posterior sclera having looser collagen fiber arrangement and lower collagen content, resulting in an elastic modulus of 0.71 ± 0.12 MPa.[34] dPS/GelMA/dSECM's mechanical property was 6.68 ± 0.48 MPa, tougher than natural sclera's. The tensile modulus of HDM is 8.18 ± 0.67 MPa. In addition, the dPS outer layer significantly altered the degradability of the overall material. In collagenase XIV, the retention rate of the dPS group and the dPS+GelMA/dSECM hydrogel group was almost 60% on day 3. In comparison, the retention rate of GelMA and GelMA/dSECM hydrogels was almost 20%, indicating improved degradation performance. On day 7, the degradation rate of the dPS/GelMA/dSECM group was limited to 42.0%. The pure GelMA/ECM hydrogel degraded rapidly, with only 20% remaining after four hours in collagenase I.[35] However, poorly degradable materials often induce the formation of a dense collagen fibrous capsule, as non-functional scar tissue. Such encapsulation may also trigger chronic inflammation or graft rejection.[36] Thus, we speculate that this design holds potential advantages of the bilayer material: the dPS layer ensures structural durability, while the degradable inner layer enables release of bioactive signals.

The inner GelMA/dSECM hydrogel also demonstrated good biological function *in vitro*. In Transwell assays, the soluble bioactive components released from the hydrogel significantly promoted HSF proliferation and migration, suggesting that dSECM-derived factors support key cellular activities. In addition, the hydrogel maintained high HSF viability when cultured in direct contact. Compared to two-dimensional culture systems, 3D hydrogels can remodel the cellular microenvironment to enhance migration and nutrient diffusion, thereby more accurately mimicking the behavior in native tissues.[37,38] The inherently porous structure of GelMA facilitates the proliferation and adhesion of fibroblasts. It also maintains high cellular viability within the 3D microenvironment.[39,40] The addition of dSECM further increased the average pore size from 36.22 ± 13.60 μm to 110.74 ± 18.49 μm. Previous research suggests that pore sizes in the range of approximately 35–137.4 μm are optimal for fibroblast proliferation, adhesion, and spreading *in vitro*,[41] while larger pores may be required *in vivo* to support vascular invasion and extensive cell migration.[42]

We found that the GelMA/dSECM hydrogel may induce directional deposition of type I collagen by IF. Snow *et al.*[43] evaluated the alignment of cardiomyocytes guided by a material scaffold using ImageJ. The Directionality plugin calculates the orientation of cell nuclei through Fourier transform or gradient analysis. It then outputs the angle of alignment to describe the directional distribution. In this study, HSFs exhibited a distinct spindle-shaped morphology, and we measured the orientation of cell nuclei as a surrogate for the alignment of the cellular long axis.[44] We observed that type I collagen was expressed

and deposited intracellularly along the long axis of the cells. Under physiological conditions, the posterior sclera surrounding the optic nerve head possesses a unique "vortex-like" or "concentric" collagen fiber architecture, which provides mechanical support around the optic nerve canal.[45] In PM, scleral collagen fibers exhibit a reduced diameter and a more parallelized arrangement, particularly in the peripheral regions away from the optic nerve.[46] However, in highly myopic eyes, the peripapillary sclera exhibits disordered collagen organization, with a significantly higher mean angular deviation (23.9 ± 18.2°) compared to normal eyes (17.9 ± 12.0°).[47] HSFs cultured on GelMA/dSECM hydrogels demonstrated enhanced alignment, as shown in Figure 4, indicating that the incorporation of dSECM better mimics the native tissue microenvironment compared to sole biological material (dPS). Building on that, the strategic design of the inner functional layer via 3D bioprinting may offer a feasible approach to enhance the efficacy of PSR surgery in the future.

Functioning as a rich reservoir of bioactive factors, ECM enables the sustained release of active molecules. Histologically, dSECM has a minimal interstitial matrix and sparse fibroblast populations. This interwoven fiber architecture imparts high elasticity and biological resilience to the tissues. Low cellular and ECM content contributes to reduced antigenicity, promoting better integration with host tissues.[48] Thus, it can establish a dynamic and pro-regenerative microenvironment to continuously guide tissue regeneration. Our bioinformatics analysis delineated a functional landscape of the dSECM proteome. This protein network centers on collagen assembly and ECM–receptor interaction. It integrates with a regulatory network for hemostasis and angiogenesis, while hub proteins (integrin alpha V and COL1A1) and bridge molecules (integrin alpha 2 and vitamin D-binding protein) mediate this integration. COL1A1 serves as a core ECM component. It helps the fibrillar network provide mechanical support and mediate cell–ECM interactions through integrins (ITGB1).[49] The integrin family functions as primary ECM receptors that maintain tissue integrity. The receptors enable mechanical force transmission and biochemical signaling by connecting the ECM to the cytoskeleton. Upon binding to ECM ligands containing RGD motifs, integrins trigger the formation of integrin-associated complexes.[50] Laminin subunit gamma-2 integrates multiple signaling networks through the ECM–receptor interaction pathway, including epidermal growth factor receptor, Phosphoinositide 3-kinase–protein kinase B, and integrin.[51-53] This integrated functionality establishes dSECM as a promising substrate supporting regenerative processes, particularly in vascularized tissue repair.

In vitro tube formation assay indicated enhanced capillary-like structure formation by HUVECs exposed to the material, and *in vivo* histological evaluation further confirmed vessel-like structures at the implant–sclera interface. Compared with the clinically used HDM, the dPS/GelMA/dSECM bilayer demonstrated better myopia control. No significant difference in scleral thickness was detected between the dPS/GelMA/dSECM group and the FDM group. This is likely due to the loosely arranged collagen fibers in the FDM group, where the measured scleral thickness included the interstitial voids within the disorganized scleral matrix. Additionally, no significant differences were observed between the dPS and dPS/GelMA/dSECM groups. We speculate that this is because the mechanical reinforcement is primarily provided by the dPS outer layer. The inner hydrogel exerts its biological functions at the histological level, as H&E and Masson's trichrome staining demonstrated collagen deposition and vessel-like structures. Han *et al.*[54] proposed that during the early stages of tissue repair, formation of new blood vessels is essential for delivering oxygen, nutrients, and immune cells. Shokrani *et al.*[55] identified that delayed neovascularization is related to cellular necrosis, impaired tissue function, and extensive fibrosis compared to native tissue. In contrast, only loose, nonfunctional fibrous encapsulation was observed in the HDM group. These findings confirm that our bilayered material restrained axial elongation and actively induced scleral regeneration and remodeling. As shown in Figure 7, at week 1, the implant was closely attached to the native sclera. Type I collagen was deposited, but the structure remained loose and disorganized. After week 2, the sclera thickened significantly and made contact with the collagen fibers. Vessel-like structures began to form around the implant. By week 4, the sclera was markedly thickened. The collagen tissue was arranged in a regular and orderly manner. These luminal structures were no longer apparent by week 4. The implant became closely associated with the surrounding scleral collagen, suggesting progressive tissue incorporation. We speculate that the observed vessel-like structures may support implant incorporation by enhancing local nutrient supply. Furthermore, dPS/GelMA/dSECM exhibited acceptable safety. In our subcutaneous implantation experiment, no significant inflammatory response was observed in guinea pig organs within eight weeks. The findings indicate that decellularization ensured low immunogenicity, coupled with the favorable biocompatibility of GelMA, which provides a strong safety foundation.

Several limitations should be acknowledged. First, the FDM guinea pig model does not recapitulate the full pathology of human PM, including PS and myopic macular degeneration. Second, the observation period was

short (eight weeks), limiting longterm safety assessment. Therefore, long-term potential surgical complications and comprehensive quality control parameters, such as implant displacement, residual detergent, and endotoxin, were not studied. Future work should address these gaps through longterm and largeanimal studies. Finally, the molecular mechanisms underlying dSECM bioactivity require direct genetic validation. The histological analyses of vascularization were primarily qualitative. Future studies about quantitative morphometry by immunohistochemical markers (e.g., CD31 for endothelial cells) are warranted for validation.

5. Conclusion

The dPS/GelMA/dSECM bilayer material integrated mechanical compatibility and biological function. It effectively controlled myopia progression and promoted scleral tissue remodeling and thickening compared to current clinical materials. These attributes underscore the potential for clinical translation.

Acknowledgments

None.

Funding

This work was supported by the Tianjin Key Medical Discipline Construction Project (TJYXZDXK-3-004A-2) and the Tianjin Municipal Health Commission Science and Technology Project (TJWJ2024QN027). The sponsor or funding organization had no involvement in any stage of this research.

Conflict of interest

The authors declare that they have no competing financial interests or personal relationships that could have appeared to influence the work reported in this paper.

Author contributions

Conceptualization: Ruihua Wei, Bin Yao, Qing He, Mengdi Chai
Data curation: Mengdi Chai, Xiu Wang, Di Wu
Formal analysis: Mengdi Chai, Xiu Wang, Di Wu
Funding acquisition: Ruihua Wei, Bin Yao, Qing He, Mengdi Chai
Investigation: Mengdi Chai, Tingting Liu, Bin Yao
Methodology: Mengdi Chai, Tingting Liu, Bin Yao
Project administration: Mengdi Chai
Validation: Mengdi Chai
Writing–original draft: Mengdi Chai
Writing–review and editing: Bin Yao, Qing He, Ruihua Wei, Xiu Wang, Di Wu

Ethics approval and consent to participate

The animal experimental protocol was approved by the Ethics Committee of Tianjin Medical University Eye Hospital (TJYY2025120271) and complied with the ARVO Statement for the Use of Animals in Ophthalmic and Vision Research.

Consent for publication

Not applicable.

Availability of data

The data that support the findings of this study are available from the corresponding author upon reasonable request.

References

1. Chen H, Liu X, Zhou X, Fu J, Wang L. Advancements in Myopic Macular Foveoschisis Research. *Ophthalmic Res*. 2024;67(1):424-434.

   doi: 10.1159/000540238

2. Németh J, Tapasztó B, Aclimandos WA, *et al*. Update and guidance on management of myopia. European Society of Ophthalmology in cooperation with International Myopia Institute. *Eur J Ophthalmol*. 2021;31(3):853-883.

   doi: 10.1177/1120672121998960

3. Modjtahedi BS, Abbott RL, Fong DS, Lum F, Tan D. Reducing the Global Burden of Myopia by Delaying the Onset of Myopia and Reducing Myopic Progression in Children: The Academy's Task Force on Myopia. *Ophthalmology*. 2021;128(6):816-826.

   doi: 10.1016/j.ophtha.2020.10.040

4. Bourke CM, Loughman J, Flitcroft DI, Loskutova E, O'Brien C. We can't afford to turn a blind eye to myopia. *Qjm*. 2023;116(8):635-639.

   doi: 10.1093/qjmed/hcz076

5. Zhang X, El Hamdaoui M, Lim S, Grytz R, Weickenmeier J. Microindentation reveals softening of the equatorial and anterior sclera during early myopia development in tree shrew eyes. *Acta Biomater*. 2025;201:446-456.

   doi: 10.1016/j.actbio.2025.05.064

6. Zhang S, Chen Y, Li Z, *et al*. Axial Elongation Trajectories in Chinese Children and Adults With High Myopia. *JAMA Ophthalmol*. 2024;142(2):87-94.

   doi: 10.1001/jamaophthalmol.2023.5835

7. Ohno-Matsui K, Wu PC, Yamashiro K, *et al*. IMI Pathologic Myopia. *Invest Ophthalmol Vis Sci*. 2021;62(5):5.

   doi: 10.1167/iovs.62.5.5

8. Xue A, Bao F, Zheng L, Wang Q, Cheng L, Qu J. Posterior scleral reinforcement on progressive high myopic young

patients. *Optom Vis Sci*. 2014;91(4):412-418.

doi: 10.1097/opx.0000000000000201

9. Zhao J, Zhao X, Jiang Y, *et al*. Incidence and Associated Factors of Myopic Maculopathy Progression after Posterior Scleral Contraction in High Myopia. *Ophthalmology*. 2026;133(4):506-514.

doi: 10.1016/j.ophtha.2025.11.002

10. Ye J, Pan AP, Zhu S, Zheng L, Lu F, Xue AQ. Posterior Scleral Contraction to Treat Myopic Foveoschisis In Highly Myopic Eyes. *Retina*. 2021;41(5):1047-1056.

doi: 10.1097/iae.0000000000002997

11. Wang P, Chen S, Liu Y, *et al*. Lowering Intraocular Pressure: A Potential Approach for Controlling High Myopia Progression. *Invest Ophthalmol Vis Sci*. 2021;62(14):17.

doi: 10.1167/iovs.62.14.17

12. Yasir ZH, Sharma R, Zakir SM. Scleral collagen cross linkage in progressive myopia. *Indian J Ophthalmol*. 2024;72(2):174-180.

doi: 10.4103/ijo.Ijo_1392_23

13. Xu Y, Chen Q, Shao Z, *et al*. Evaluation of new robust silk fibroin hydrogels for posterior scleral reinforcement in rabbits. *Front Bioeng Biotechnol*. 2023;11:1211688.

doi: 10.3389/fbioe.2023.1211688

14. Jobling AI, Gentle A, Metlapally R, McGowan BJ, McBrien NA. Regulation of scleral cell contraction by transforming growth factor-beta and stress: competing roles in myopic eye growth. *J Biol Chem*. 2009;284(4):2072-2079.

doi: 10.1074/jbc.M807521200

15. Zhou XB, Huang YF, Wu ZH, Jiao XJ. Niu xin bao sheng wu bu pian dui hou gong mo jia gu qu de sheng wu li xue te xing ji qi zuo yong ji zhi [Biomechanical properties and mechanism of bovine pericardium biological patch on the posterior scleral reinforcement area]. *Med J Chin People Armed Police Forces*. 2015;(6):609-612. [In Chinese]

doi: 10.3969/j.issn.1004-3594.2015.06.023

16. Wang T, Zhang JS. Yi ti tuo xi bao zhen pi wang mo hou gong mo jia gu shu hou zu zhi rong he xing ji bFGF biao da de bian hua [Changes in histocompatibility and bFGF expression after posterior scleral reinforcement using allogeneic acellular dermal matrix]. *Recent Adv Ophthalmol*. 2015;35(10):921-923. [In Chinese]

doi: 10.13389/j.cnki.rao.2015.0251

17. Ma J, Wu F, Liu Z, *et al*. Biomechanical Considerations of Patching Material for Posterior Scleral Reinforcement Surgery. *Front Med*. 2022;9:888542.

doi: 10.3389/fmed.2022.888542

18. Zwirner J, Ondruschka B, Scholze M, Schulze-Tanzil G, Hammer N . Mechanical and morphological description of human acellular dura mater as a scaffold for surgical reconstruction. *J Mech Behav Biomed Mater*. 2019;96:38-44.

doi: 10.1016/j.jmbbm.2019.04.035

19. Khurana D, Suresh A, Nayak R, *et al*. Biosubstitutes for dural closure: Unveiling research, application, and future prospects of dura mater alternatives. *J Tissue Eng*. 2024;15:20417314241228118.

doi: 10.1177/20417314241228118

20. Muniz NO, Baudequin T. Biomimetic and Nonbiomimetic Approaches in Dura Substitutes: The Influence of Mechanical Properties. *Tissue Eng Part B Rev*. 2025;31(2):174-189.

doi: 10.1089/ten.TEB.2024.0079

21. Hui J, Nie X, Wei P, *et al*. 3D printed fibroblast-loaded hydrogel for scleral remodeling to prevent the progression of myopia. *J Mater Chem B*. 2024;12(10):2559-2570.

doi: 10.1039/d3tb02548a

22. Zhong T, Yi H, Gou J, *et al*. A wireless battery-free eye modulation patch for high myopia therapy. *Nat Commun*. 2024;15(1):1766.

doi: 10.1038/s41467-024-46049-6

23. Sun Y, Yu K, Nie J, *et al*. Modeling the printability of photocuring and strength adjustable hydrogel bioink during projection-based 3D bioprinting. *Biofabrication*. 2021;13(3):035032.

doi: 10.1088/1758-5090/aba413

24. Gaglio CG, Baruffaldi D, Pirri CF, Napione L, Frascella F. GelMA synthesis and sources comparison for 3D multimaterial bioprinting. *Front Bioeng Biotechnol*. 2024;12:1383010.

doi: 10.3389/fbioe.2024.1383010

25. Im GB, Lin RZ. Bioengineering for vascularization: Trends and directions of photocrosslinkable gelatin methacrylate hydrogels. *Front Bioeng Biotechnol*. 2022;10:1053491.

doi: 10.3389/fbioe.2022.1053491

26. Madl CM, Heilshorn SC. Bioorthogonal Strategies for Engineering Extracellular Matrices. *Adv Funct Mater*. 2018;28(11):1706046.

doi: 10.1002/adfm.201706046

27. Lian L, Xie M, Luo Z, *et al*. Rapid Volumetric Bioprinting of Decellularized Extracellular Matrix Bioinks. *Adv Mater*. 2024;36(34):e2304846.

doi: 10.1002/adma.202304846

28. Cai D, Weng W. Development potential of extracellular matrix hydrogels as hemostatic materials. *Front Bioeng Biotechnol*. 2023;11:1187474.

doi: 10.3389/fbioe.2023.1187474

29. Wang F, Zhao L, Li H, *et al*. Scleral defect repair

using decellularized porcine sclera in a rabbit model. *Xenotransplantation*. 2020;27(6):e12633.

doi: 10.1111/xen.12633

30. Pei ZW, Wang JZ. Yuan wei 3D sheng wu da yin ji shu zai gu he ruan gu sun shang xiu fu zhong de yan jiu jin zhan [Research progress of in-situ 3D bioprinting technology for repairing bone and cartilage injuries]. *Zhongguo Xiu Fu Chong Jian Wai Ke Za Zhi*. 2022;36(4):487-494. [In Chinese]

doi: 10.7507/1002-1892.202111043

31. Cheng W, Huang Y, Dai J, *et al*. Endotoxin, not DNA, determines the host response and tissue regeneration behavior of acellular biologic scaffolds. *Acta Biomater*. 2025;195:157-168.

doi: 10.1016/j.actbio.2025.02.010

32. Jiang L, Zhao B, Li Q, *et al*. A Self-Generated Electricity-Driven Sclera reinforcement bionic piezoelectric patch for Management of High Myopia. *J Nanobiotechnology*. 2025;23(1):470.

doi: 10.1186/s12951-025-03493-w

33. Shirzadi H, Zohoor H, Naserkhaki S. Biomechanical simulation of eye-airbag impacts during vehicle accidents. *Proc Inst Mech Eng H*. 2018;232(7):699-707.

doi: 10.1177/0954411918778063

34. Wang C, Xie Y, Wang G. The elastic modulus and collagen of sclera increase during the early growth process. *J Mech Behav Biomed Mater*. 2018;77:566-571.

doi: 10.1016/j.jmbbm.2017.10.024

35. Zhang M, Yang F, Han D, *et al*. 3D bioprinting of corneal decellularized extracellular matrix: GelMA composite hydrogel for corneal stroma engineering. *Int J Bioprint*. 2023;9(5):774.

doi: 10.18063/ijb.774

36. Ward NA, Hanley S, Tarpey R, *et al*. Intermittent actuation attenuates fibrotic behaviour of myofibroblasts. *Acta Biomater*. 2024;173:80-92.

doi: 10.1016/j.actbio.2023.11.017

37. Boere KW, Visser J, Seyednejad H, *et al*. Covalent attachment of a three-dimensionally printed thermoplast to a gelatin hydrogel for mechanically enhanced cartilage constructs. *Acta Biomater*. 2014;10(6):2602-2611.

doi: 10.1016/j.actbio.2014.02.041

38. Benton JA, DeForest CA, Vivekanandan V, Anseth KS. Photocrosslinking of gelatin macromers to synthesize porous hydrogels that promote valvular interstitial cell function. *Tissue Eng Part A*. 2009;15(11):3221-3230.

doi: 10.1089/ten.TEA.2008.0545

39. Bilici C, Altunbek M, Afghah F, Tatar AG, Koc B. Embedded 3D Printing of Cryogel-Based Scaffolds. *ACS Biomater Sci Eng*. 2023;9(8):5028-5038.

doi: 10.1021/acsbiomaterials.3c00751

40. Shi M, Xu Q, Ding L, *et al*. Cell Infiltrative Inner Connected Porous Hydrogel Improves Neural Stem Cell Migration and Differentiation for Functional Repair of Spinal Cord Injury. *ACS Biomater Sci Eng*. 2022;8(12):5307-5318.

doi: 10.1021/acsbiomaterials.2c01127

41. Shamloo A, Sarmadi M, Aghababaie Z, Vossoughi M. Accelerated full-thickness wound healing via sustained bFGF delivery based on a PVA/chitosan/gelatin hydrogel incorporating PCL microspheres. *Int J Pharm*. 2018;537(1-2):278-289.

doi: 10.1016/j.ijpharm.2017.12.045

42. Fu J, Wiraja C, Muhammad HB, Xu C, Wang DA. Improvement of endothelial progenitor outgrowth cell (EPOC)-mediated vascularization in gelatin-based hydrogels through pore size manipulation. *Acta Biomater*. 2017;58:225-237.

doi: 10.1016/j.actbio.2017.06.012

43. Snow F, O'Connell C, Elbourne A, *et al*. High resolution melt electro-written scaffolds promote alignment of human skeletal muscle cells. *Biofabrication*. 2025;17(3):035013.

doi: 10.1088/1758-5090/add960

44. Saporito S, Panzetta V, Netti PA. Time and space modulation of substrate curvature to regulate cell mechanical identity. *Acta Biomater*. 2024;186:300-315.

doi: 10.1016/j.actbio.2024.08.006

45. Lu H, Wu Y, Xiong J, *et al*. Whorl-Like Collagen Fiber Arrangement Around Emissary Canals in the Posterior Sclera. *Invest Ophthalmol Vis Sci*. 2025;66(3):35.

doi: 10.1167/iovs.66.3.35

46. Hoerig C, McFadden S, Hoang QV, Mamou J. Biomechanical changes in myopic sclera correlate with underlying changes in microstructure. *Exp Eye Res*. 2022;224:109165.

doi: 10.1016/j.exer.2022.109165

47. Markov PP, Eliasy A, Pijanka JK, *et al*. Bulk changes in posterior scleral collagen microstructure in human high myopia. *Mol Vis*. 2018;24:818-833.

48. Crapo PM, Gilbert TW, Badylak SF. An overview of tissue and whole organ decellularization processes. *Biomaterials*. 2011;32(12):3233-3243.

doi: 10.1016/j.biomaterials.2011.01.057

49. Saraswathibhatla A, Indana D, Chaudhuri O. Cell-extracellular matrix mechanotransduction in 3D. *Nat Rev Mol Cell Biol*. 2023;24(7):495–516.

doi: 10.1038/s41580-023-00583-1

50. Chastney MR, Kaivola J, Leppanen VM, Ivaska J. The role and regulation of integrins in cell migration and invasion.

Nat Rev Mol Cell Biol. 2025;26(2):147-167.

doi: 10.1038/s41580-024-00777-1

51. Kirtonia A, Pandey AK, Ramachandran B, *et al*. Overexpression of laminin-5 gamma-2 promotes tumorigenesis of pancreatic ductal adenocarcinoma through EGFR/ERK1/2/AKT/mTOR cascade. *Cell Mol Life Sci*. 2022;79(7):362.

doi: 10.1007/s00018-022-04392-1

52. Chen XY, Wang MY, Shu X, Li J, Tang R, Liu XQ. Matrix-bound EGF promotes malignant phenotypes of breast cancer organoids in the biomimetic ECM of alginate. *Mater Today Bio*. 2025;32:101818.

doi: 10.1016/j.mtbio.2025.101818

53. Wang D, Keyoumu K, Yu R, *et al*. Extracellular matrix marker LAMC2 targets ZEB1 to promote TNBC malignancy via up-regulating CD44/STAT3 signaling pathway. *Mol Med*. 2024;30(1):61.

doi: 10.1186/s10020-024-00827-6

54. Han C, Barakat M, DiPietro LA. Angiogenesis in Wound Repair: Too Much of a Good Thing? *Cold Spring Harb Perspect Biol*. 2022;14(10):a041225.

doi: 10.1101/cshperspect.a041225

55. Shokrani H, Shokrani A, Sajadi SM, *et al*. Cell-Seeded Biomaterial Scaffolds: The Urgent Need for Unanswered Accelerated Angiogenesis. *Int J Nanomedicine*. 2022;17:1035-1068.

doi: 10.2147/ijn.S353062